NJC

Accepted Manuscript

This is an *Accepted Manuscript*, which has been through the Royal Society of Chemistry peer review process and has been accepted for publication.

Accepted Manuscripts are published online shortly after acceptance, before technical editing, formatting and proof reading. Using this free service, authors can make their results available to the community, in citable form, before we publish the edited article. We will replace this *Accepted Manuscript* with the edited and formatted *Advance Article* as soon as it is available.

You can find more information about *Accepted Manuscripts* in the Information for Authors.

Please note that technical editing may introduce minor changes to the text and/or graphics, which may alter content. The journal's standard Terms & Conditions and the Ethical guidelines still apply. In no event shall the Royal Society of Chemistry be held responsible for any errors or omissions in this *Accepted Manuscript* or any consequences arising from the use of any information it contains.

ROYAL SOCIETY OF CHEMISTRY

www.rsc.org/njc

New Journal of Chemistry

RSC Publishing

PAPER

A General Method for Type I and Type II g-C_3N_4/g-C_3N_4 Metal-Free Isotype Heterostructures with Enhanced Visible Light Photocatalysis

Received (in XXX, XXX) Xth XXXXXXXXX 20XX,

Accepted Xth XXXXXXXXX 20XX

DOI: 10.1039/b000000x

www.rsc.org/

Fan Dong [a,*], Zilin Ni [a], Peidong Li [a], Zhongbiao Wu [b]

[a] *Chongqing Key Laboratory of Catalysis and Functional Organic Molecules, College of Environmental and Biological Engineering, Chongqing Technology and Business University, Chongqing, 400067, China*

[b] *Department of Environmental Engineering, Zhejiang University, Hangzhou, Zhejiang 310027, China*.

Abstract: In order to address the fast charge recombination of pristine g-C_3N_4, easily available composite precursors such as dicyandiamide (melamine) and urea were used and thermally treated, in situ creating Type I and Type II g-C_3N_4/g-C_3N_4 metal-free isotype heterostructures. The construction of these heterostructure was based on different band-alignment patterns (staggered and straddled band alignments). The confirmation of isotype g-C_3N_4/g-C_3N_4 heterostructures was based on X-ray diffration, photoluminescence, transmission electron microscopy, and valence band X-ray photoelectron spectroscopy. For g-C_3N_4/g-C_3N_4 heterostructures from dicyandiamide and urea (Type II, staggered band alignments) heterostructure under visible light, the photogenerated electrons in the conduction band of CN-D (g-C_3N_4 from dicyandiamide) could transfer to the conduction band of CN-U (g-C_3N_4 from urea) driven by offset of 0.04 eV, whereas the photogenerated holes could transfer from CN-U to CN-D driven by valence band offset of 0.36 eV, thus photogenerated electrons and holes could be separated effectively. For g-C_3N_4/g-C_3N_4 heterostructures from melamine and urea (Type I, straddled band alignments) heterostructure, the photo-induced electrons could transfer from CN-U to CN-M (g-C_3N_4 from melamine) driven by conduction band offset of 0.17 eV, while photogenerated holes could not be transported from one side to another side, also promoting the separation of photo-induced electrons and holes. The intrinsic drawback of fast charge recombination of pristine g-C_3N_4 was overwhelmed by formation of Type I and Type II g-C_3N_4/g-C_3N_4 heterostructures. For the removal of ppb-level NO in air, the Type I and Type II g-C_3N_4 based heterostructures demonstrated highly enhanced photocatalytic activity and stability in comparison with g-C_3N_4 alone, which could be directly ascribed to the promoted the charge separation. The rational design and construction of Type I and Type II isotype heterojunction was general and powerful for the development of efficient visible-light photocatalysts with potential large scale environmental and energetic applications. The present work could also enrich new types of visible-light heterostructured photocatalysts, which may also find wide applications in other areas.

Keywords: Carbon nitride photocatalysis; Type I and Type II heterostructures; Composite precursors; Charge separation and transfer; band alignment.

1. Introduction

A wave of visible-light photocatalysis has hit the world, as it provides a green and potential route for wide applications such as environmental remediation, clean energy production, carbon fixation and final chemical synthesis.[1-10] It is demonstrated that the photocatalytic performance of semiconductors is predominantly controlled by the intrinsic physicochemical properties, including band gap structure, charge separation kinetics, surface areas, and morphology.[1-5] The band gap structure of semiconductors, which could determine the position of valence band and conduction band, light absorption spectra, and charge transfer, is a key factor.[1-3,5-8]

Recently, Wang et al discovered polymeric graphitic carbon nitride (g-C_3N_4) as a metal free visible light photocatalyst.[11] In general, the g-C_3N_4 can be prepared by thermal condensation of nitrogen-rich precursors, such as cyanamide, dicyandiamide, trithiocyanuric acid, melamine, urea and thiourea.[12-22] However, the photocatalytic performance of g-C_3N_4 has been restricted by the fast charge recombination. To improve the photocatalytic performance of g-C_3N_4, various strategies have been developed, such as doping, formation of heterostructures, metal deposition and nanostructure engineering. The band alignment of two semiconductors with well-matched band structure is generally employed to promote the separation of charge at

the interfaces of the two components, subsequently enhancing the photocatalytic performance.[23-30] Several kinds of g-C_3N_4-based heterojunction systems have been developed by coupling g-C_3N_4 with other types of inorganic photocatalysts.[23-30] Successful examples include inorganic-organic heterojunctions of graphene/g-C_3N_4, Au/g-C_3N_4, TiO_2/g-C_3N_4, MoS_2/g-C_3N_4, TaON/g-C_3N_4, ZnO/g-C_3N_4, Bi_2WO_6/g-C_3N_4, CdS/g-C_3N_4, WO_3/g-C_3N_4, BiOBr/g-C_3N_4, $(BiO)_2CO_3$/C_3N_4, $ZnWO_4$/C_3N_4, N-doped ZnO/g-C_3N_4 and three component nanowires semiconductor composite CF(carbon fibers)–WO_3-Pt-CdS.[23-35] Recently, the band alignment strategy is further advanced by formation of phase heterojunction between two different crystal phases of a single semiconductor, such as anatase-rutile phase TiO_2 heterojunction,[36-37] α-β-phase Ga_2O_3 heterojunction.[38] The development and performance of these heterojunction relies largely on the band structure of the well-matched semiconductors.[39]

The band-alignment design of semiconductors is generally adopted to promote the dissociation of excitons and facilitate the subsequent collection and separation of charge carriers at the interface of two semiconductors, minimizing charge recombination.[40] Depending on the band alignments pattern of semiconductors, heterojunction can be divided into three types, namely straddled gap (type I), staggered gap (type II) or broken gap (type III). Such band alignments can effectively promote the separation of charge carriers at the junction interface.[41-42]

In early times, much attention has been focused on the study of type I heterostructures such as GaAs/GaAIAs,[43] InGaAsP/InP,[43] CdSe/ZnS,[44] CdSe/ZnSe[45] and so on. Subsequently, some type-II systems are found, including CdTe/CdSe,[46] CdSe/ZnTe,[47] CdS/ZnSe,[48] ZnTe/CdS,[49] ZnO/CdS,[50] InP/GaAs.[51] The morphologies of type-II heterojunction range from core/shell geometrics to linear heterostructures, nanobarbells and tetrapods.[46] Of particular interest are type-II heterostructures, where the relative band alignment of their constituent semiconductor materials promotes a spatial separation of the electron and hole following photoexcitation, a highly desirable property for photovoltaic applications[46] and nontoxic biomedical applications.[46] In addition, type-II heterojunction such as CdTe/CdSe can be effectively used for in vivo imaging,[52] and strained-silicon/strained-germanium type-II staggered heterojunctions can be utilized to tunnel field-effect transistors.[53] There are also the s-SWCNT/polymer type-II nanohybrid as uncooled infrared detectors,[54] and bright, water-soluble near IR-emitting CdSe/CdTe/ZnSe core/shell/shell type-II/type-I nanocrystals, with highly photoluminescent quantum yield.[55]

Very recently, Wang et al prepared g-C_3N_4 based CNS-CN (sulfur-mediated carbon nitride-carbon nitride) isotype metal-free heterojunction with enhanced visible-light activity on the basis that the g-C_3N_4 from different precursors has different band structure.[56] The slight differences in the band structure between two CNS and CN enable the formation of isotype nanojunction, leading to the enhanced photocatalytic activity arising from promoted charge separation.[40-42,56] We have developed a facile in situ method to construct type II g-C_3N_4/g-C_3N_4 metal-free isotype heterojunction with molecular composite precursors of urea and thiourea, which can greatly promote the charge separation and subsequently enhance the photocatalytic activity.[57]

g-C_3N_4 prepared from different types of precursors have different band structure in the positions conduction band and conduction band, which is caused by different degree of polycondensation.[58] By coupling g-C_3N_4 with different band structure, there are great potentials to construct g-C_3N_4 mental-free heterostructure with different band alignment patterns. The construction of g-C_3N_4/g-C_3N_4 heterojunction could provide an alternative novel route to address the intrinsic drawbacks of g-C_3N_4 for enhanced photocatalysis without relying on external semiconductors.[57-58] In the present work, different easily available composite precursors such as dicyandiamide (melamine) and urea were used and treated under the same thermal conditions, which resulted in the creation of Type I and Type II g-C_3N_4/g-C_3N_4 metal-free isotype heterojunction. We found the as-prepared g-C_3N_4/g-C_3N_4 Type I and Type II heterojunctions demonstrated conspicuous photocatalytic superiority over g-C_3N_4 alone, which could be ascribed to the promoted charge separation benefiting from the unique heterojunctions. The present work has demonstrated the rational design and construction of Type I and Type II isotype heterojunction for the development of efficient visible-light photocatalysts with potential large scale environmental and energetic applications.

2. Experimental

2.1. Construction of Type-I and Type-II g-C_3N_4/g-C_3N_4 metal-free heterostructures.

All chemicals used in this study were analytical grade and were used without further treatment. The typical synthesis strategies were as following. To begin with, 6 g of dicyandiamide (melamine) and 6 g of urea were mixed in 30 mL water in an alumina crucible. Then, the solution of dicyandiamide (melamine) and urea was dried at 60 ^oC overnight to get the composite precursors. Next, the composite precursors, in semiclosed alumina crucible with a cover, were heated to 550 ^oC at a heating rate of 15 ^oC min^{-1} in a muffle furnace and maintained for 3 h. Finally, the alumina crucible was cooled down to room temperature after the reaction. The as-obtained g-C_3N_4/g-C_3N_4 metal-free heterojunction was collected for further use. The gases released during the thermal treatment were absorbed by dilute alkaline solution. For comparison, 12 g of dicyandiamide (melamine) and 12 g of urea were treated separately under the same thermal conditions. For convenience, the g-C_3N_4 samples from dicyandiamide, urea and melamine precursors were labeled as CN-D, CN-U and CN-M, respectively. The Type-II g-C_3N_4/g-C_3N_4 heterojunction prepared from dicyandiamide and urea was labeled as CN-DU. The Type-I g-C_3N_4/g-C_3N_4 heterojunction obtained from melamine and urea was labeled as CN-MU.

2.2. Structural Characterization Methods.

X-ray diffraction with Cu Kα radiation (XRD model D/max RA, Japan) was utilized to analyze the crystal phase at a scan rate of 0.01^o 2θ/s with a scan range of 2θ from 5^o to 80^o. The morphology and structure of samples were obtained from transmission electron microscopy (TEM: JEM-2010, Japan). Functional groups and chemical bonds were exhibited by FT-IR spectra on a Nicolet Nexus spectrometer with samples embedded in KBr pellets. The UV-vis diffuse reflection spectra was measured for the dry-pressed disk samples using a Scan UV-vis spectrophotometer (UV-vis DRS UV-2450, Shimadzu, Japan) equipped with an integrating sphere assembly and $BaSO_4$ as reflectance sample. Prior to measurements, all samples were degassed at 150 ^oC for 12 h, then nitrogen adsorption-desorption isotherms were measured by a nitrogen adsorption apparatus (ASAP 2020, USA). The photoluminescence spectra was measured with a fluorescence spectrophotometer (F-7000, Japan) using a Xe lamp as excitation source with optical filters.

2.3. Evaluation of Visible Light Photocatalytic activity.

The photocatalytic activity was investigated by removal of NO at ppb levels in a continuous flow reactor at ambient temperature. The rectangular reactor, whose volume was 4.5 L (30 cm × 15 cm × 10 cm), was made of stainless steel and covered with Saint-Glass, with a 150 W commercial tungsten halogen lamp vertically hung outside. A

UV cutoff optical filter (420 nm) was adopted to remove UV light in the light beam. Firstly, with 0.1 g sample, a small beaker was added 30 mL of distilled water into and ultrasonicated for 10 min. Then the aqueous suspension was coated onto the glass dishes, drying at 60 °C and then cooled to room temperature before photocatalytic testing. For each photocatalytic activity test, each of two sample dishes (with a diameter of 12.0 cm), contains 0.1 g photocatalyst powders were placed in the center of the reactor. The NO gas was acquired from a compressed gas cylinder at a concentration of 100 ppm of NO (N_2 balance). The initial concentration of NO was diluted to about 600 ppb by the air stream. By passing the zero air streams through a humidification chamber, the desired relative humidity (RH) level of the NO flow was controlled at 50%. The gas streams were premixed completely by a gas blender, and the flow rate was controlled at 2.4 L/min by a mass flow controller. Once the adsorption-desorption reached equilibrium, the lamp was turned on. The concentration of NO was continuously measured by a chemiluminescence NO analyzer (Thermo Environmental Instruments Inc., 42i-TL), which monitors NO and NO_2 with a sampling rate of 1.0 L/min. The removal ratio (η) of NO was calculated as η (%) = (1-C/C_0) × 100%, where C and C_0 are concentrations of NO in the outlet steam and the feeding stream, respectively.

3. Results and discussion

Easily available composite precursors of dicyandiamide (melamine) and urea were used and thermally treated to construct Type I and Type II g-C_3N_4/g-C_3N_4 metal-free isotype heterostructures based on different band-alignment patterns.

3.1. Conformation of g-C_3N_4/g-C_3N_4 metal-free isotype heterostructures.

The XRD patterns of all the samples are presented in Fig. 1, which confirms the formation of graphitic stacking C_3N_4 layers for all the samples.[59] Two peaks can be observed in all of the g-C_3N_4 or g-C_3N_4/g-C_3N_4 heterojunction samples from different precursors. The (100) peaks around 13.0° correspond to the in-plane tri-s-triazine units (Fig. 1a and 1c). The strongest peaks around 27.5° are indexed to the (002) plane, which demonstrates the graphite-like stacking of the conjugated aromatic units. As shown in Fig. 1b, the dominant (002) peak of CN-DU is located between CN-D and CN-U, implying the construction of CN-D/CN-U heterostructure. Similarly, the (002) peak of CN-MU is located between CN-M and CN-U (Fig. 1d). Benefiting from the use of composite precursors, the electronic interplay of between CN-D and CN-U, CN-M and CN-U could take place at the atomic level.

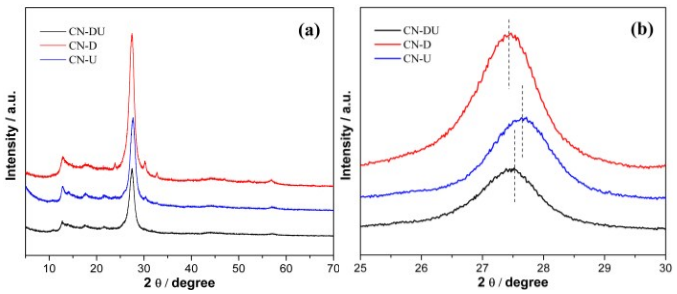

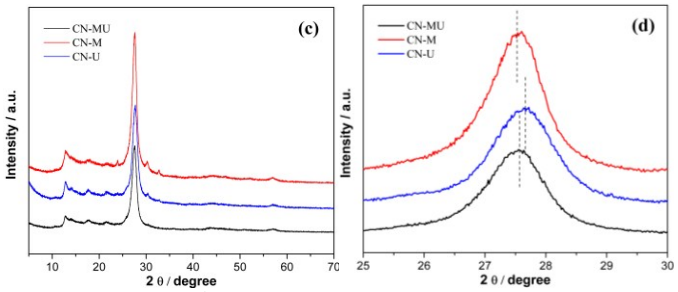

Fig. 1 XRD patterns of CN-D, CN-U, CN-DU (a, b), and CN-M, CN-U, CN-MU (c, d)

The SEM images of all the samples can be found in Fig. S1. It is difficult to identify the different components in the g-C_3N_4/g-C_3N_4 heterostructures as they show similar surface morphology. So, TEM is further used to reveal the morphological structure of g-C_3N_4/g-C_3N_4 heterostructures, as shown in Fig. 2. We can observe that CN-D is composed of bulk and thick layers (Fig. 2a) and CN-U consists of thin paper-fold nanosheets (Fig. 2b). According to the differences in morphology and microstructure between CN-D and CN-U, we can differentiate CN-D from CN-U in CN-DU heterostructure (Fig. 2c), although they are in close contact. The TEM images of CN-M and CN-U are presented in Fig. 2d and 2e. The differences between them are obvious, which could make the recognition of CN-M and CN-U in CN-MU (Fig. 2f) heterostructure feasible. The successful construction of CN-D/CN-U and CN-M/CN-U metal-free isotype heterostructures can be achieved by using composite precursors.

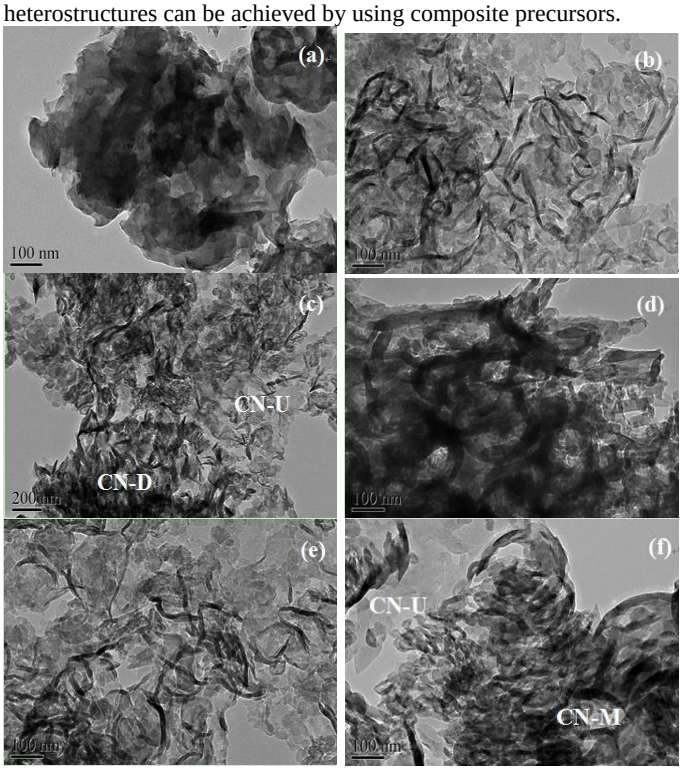

Fig. 2 TEM images of CN-D (a), CN-U (b), CN-DU (c), CN-M (d), CN-U (e) and CN-MU (f).

Fig. 3 illustrates the nitrogen adsorption-desorption isotherms and pore-size distribution (PSD) curves from all the samples. As shown in Fig. 3a and 3c, the isotherms of all samples can be classified to type IV, indicating the presence of mesopores.[60-61] The hysteresis loops are of type H3, ascribing to the slit-shaped pores which is consistent with TEM nanosheets image (Fig. 2). Compared with CN-D and CN-M, the hysteresis loop of CN-U owns the lowest pressure and the largest

areas. As the additional oxygen in the urea plays a crucial role in enlarging the surface area of g-C_3N_4,[18] CN-U shows the superiority in construction of metal free heterostructure. The hysteresis loop of CN-DU (CN-MU) is between CN-D (CN-M) and CN-U, further confirming the formation of heterostructures in CN-DU and CN-MU.

The surface areas and pore parameters are listed in Table 1. The surface areas and pore volumes of CN-DU and CN-MU are located between the pristine samples. The PSD curves show multi-modal peaks, as also shown in Table 1. The small mesopores can be ascribed to the pores within the layers, and large mesopores pores from the stack of the layers.

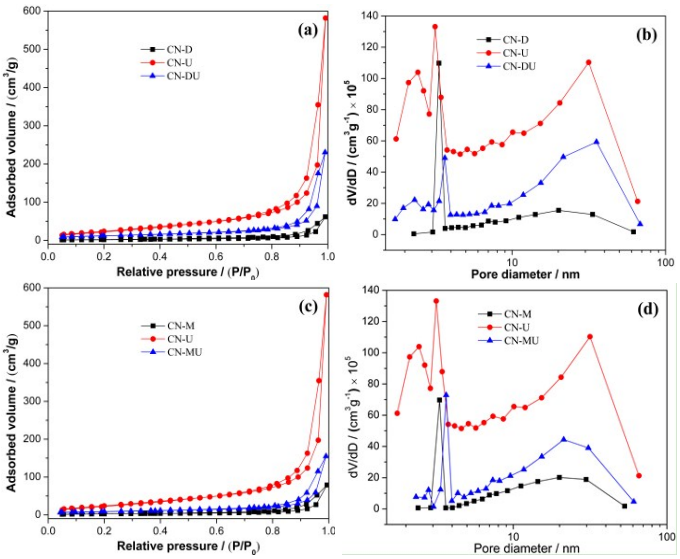

Fig. 3 N_2 adsorption-desorption isotherms (a) and the corresponding pore size distribution curves (b) of all the samples.

Table 1 Summary of the specific surface areas, pore parameters for all the samples.

Samples	S_{BET} (m^2/g)	Total volume (cm^3/g)	Peak diameter(nm)
CN-D	7	0.096	3.3/20.1
CN-M	10	0.12	3.3/20.0
CN-U	91	0.90	2.4/3.2/31.6
CN-DU	45	0.36	2.3/3.6/35.5
CN-MU	32	0.24	2.8/3.7/21.3

3.2 Chemical Composition.

As shown in Fig. 4, the FT-IR spectra curves of CN-D, CN-U, CN-DU, CN-DU-used, CN-M, CN-MU and CN-MU-used present the same characteristics. Ascribing to the breathing mode of the triazine units, the absorption bands of all the g-C_3N_4 samples are in the region 800-880 cm^{-1}. The typical vibrations C-N heterocycles show the peaks at 1200-1480 cm^{-1}. Due to the presence of C=N bonds, the peaks in the region of 1570-1640 cm^{-1} can be observed. And the broad band in the range 3000-3600 cm^{-1} is consistent with the uncondensed amine groups and surface adsorbed water molecules.[60-61]

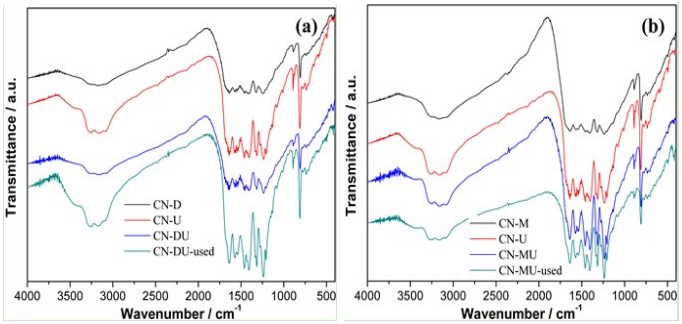

Fig. 4 FT-IR spectra for all the samples.

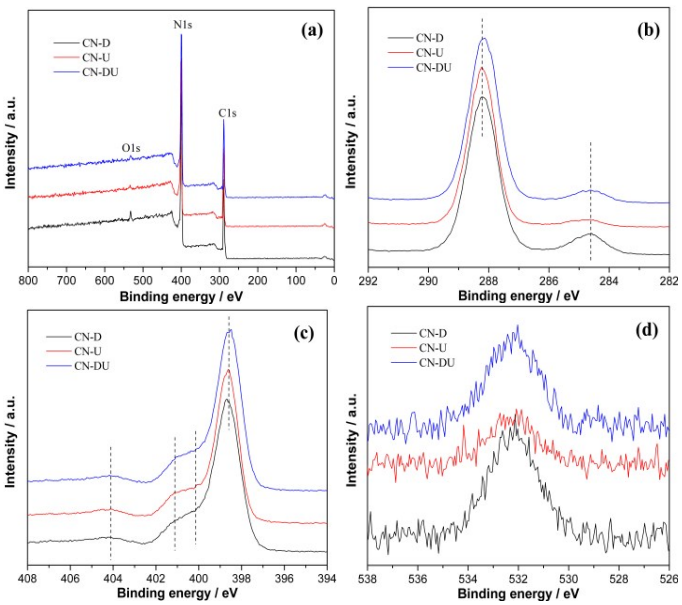

Fig. 5 XPS spectra of CN-D, CN-U, and CN-DU, (a) survey, (b) C1s, (c) N1s, and (d) O1s.

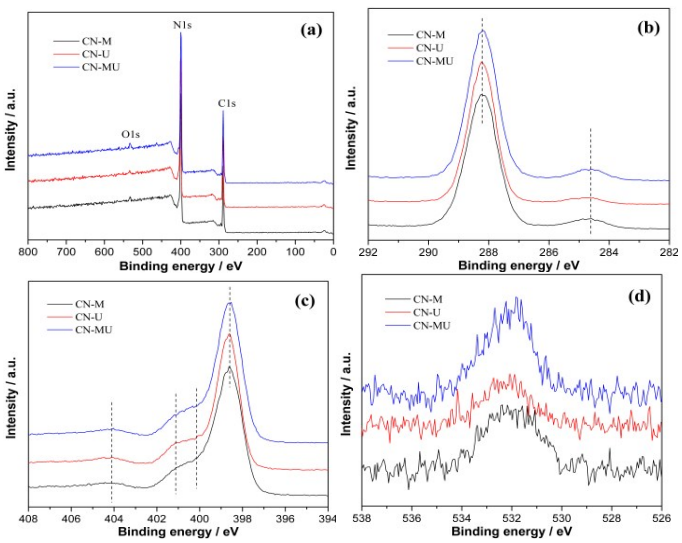

Fig. 6 XPS spectra of CN-M, CN-U, and CN-MU, (a) survey, (b) C1s, (c) N1s, and (d) O1s.

The chemical states of the elements of the samples were investigated by XPS, as shown in Fig. 5 and Fig. 6. The full survey spectra (Fig. 5a and Fig. 6a) indicate that all the samples are composed C, N and O elements. The C1s spectra in Fig. 5b and 6b

represent two peaks at the binding energies of 284.8 and 288.1 eV, respectively. The peak located at 284.8 eV is assigned to adventitious carbon species, and the peak at 288.1 eV is assigned to the tertiary carbon C-$(N)_3$ in the g-C_3N_4 lattice.[60-62] The peaks for N1s region in Fig. 5c and 6c can be fitted into four peaks, which can be ascribed to C-N-C (398.8 eV), tertiary nitrogen N-$(C)_3$(400.1eV), N-H groups (401.2eV), and π-excitations (404.3 eV), respectively.[60-62] Fig. 5d and 6d shows the O 1s peak at 532 eV which is mainly assigned to the adsorbed H_2O on the surface.

3.3 Working mechanisms of CN-DU and CN-MU metal-free heterostructures.

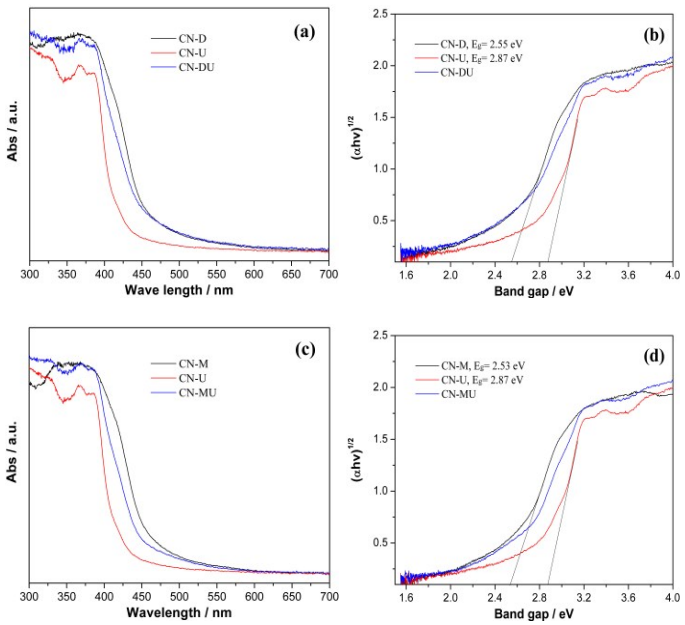

Fig. 7 UV-vis DRS (a, c) and plots of (αhv)1/2 vs. photon energy (b, d) of all the samples.

Fig. 7a and 7c shows the UV-vis DRS for all the samples. It can be seen that the g-C_3N_4 prepared from dicyandiamide, melamine and urea has different absorption edges, which is consistent with previous report.[60-62] By thermal condensation of composite precursors of dicyandiamide (melamine) and urea under the same conditions, CN-DU and CN-MU heterostructures can be constructed. The optical absorption edge of CN-DU is located between CN-D and CN-U, and absorption edge of CN-MU is positioned between CN-M and CN-U, which is a typical property of semiconductor-based heterostructures. By plots of $(\alpha h\nu)^{1/2}$ vs. photon energy, the band gap energy can be determined (Fig. 7b and 7d). The band gap of CN-D, CN-M and CN-U is 2.55, 2.53 and 2.87 e V, respectively. The different band gap energy between CN-D (CN-M) and CN-U provide good opportunity for construction of metal free heterostructure between g-C_3N_4 and g-C_3N_4.

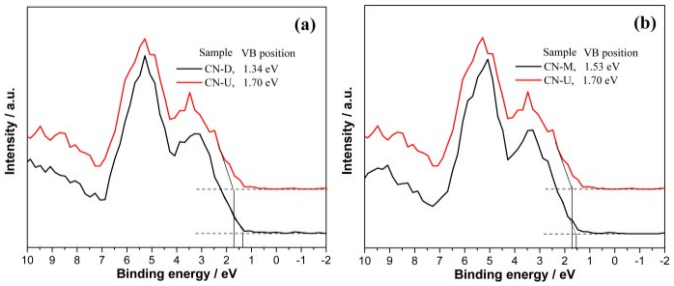

Fig. 8 VB XPS spectra for CN-D, CN-M and CN-U.

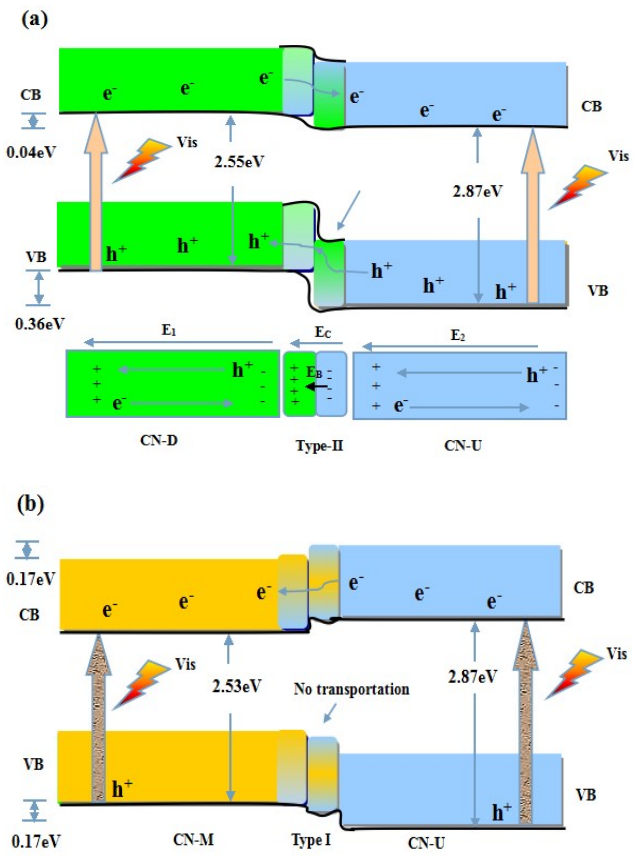

Fig. 9 Illustration of type I and type II g-C_3N_4/ g-C_3N_4 heterostructures working under visible light irradiation.

The valence band (VB) position of semiconductor can be determined by VB XPS, as depicted in Fig. 8. The VB position of CN-D, CN-U and CN-M are determined to be 1.34, 1.70 and 1.53 eV, respectively. Considering the band gap energy from Fig. 7, the CB position can be calculated, as listed in Table 2.

For CN-DM system, the VB position of CN-U (1.70 eV) is more positive than that of CN-D (1.34). And the CB position of CN-D (-1.21 eV) is more negative than that of CN-U (-1.17). By in situ coupling CN-D and CN-U, a g-C_3N_4/g-C_3N_4 isotype heterostructure will be formed. The CN-DU heterostructure belongs to type II heterostructure owning band gaps that form a staggered alignment.[41-42] For CN-MU system, the CB position of CN-U (-1.17 eV) is more negative than that of CN-M (-1.0 eV). However, the VB position of CN-M (1.53 eV) is more negative than that of CN-U (1.70 eV). In this coupling way, the CN-MU heterostructure can be classified to type I heterostructure with a straddled band alignment.[41-42] Ascribing to the distinct differences in band structure of g-C_3N_4 from different

precursors, the construction of g-C_3N_4-based isotype heterostructures with well-matched band structure can be constructed by selecting appropriate composites precursors.

Table 2 The determined VB position, CB position, band gap energy, and NO removal ratio for the as-prepared samples.

Sample	VB position (eV)	CB position (eV)	Band gap E_g (eV)	NO removal ratio η (%)
CN-D	1.34	-1.21	2.55	22.0
CN-U	1.70	-1.17	2.87	29.6
CN-DU	-	-	-	39.3
CN-M	1.53	-1.0	2.53	26.8
CN-U	1.70	-1.17	2.87	29.6
CN-MU	-	-	-	41.3

Fig. 9 illustrate the working mechanisms of type-II and type-I g-C_3N_4/ g-C_3N_4 heterostructures under visible light irradiation. For CN-DU heterojunction (Fig. 9a), with visible-light irradiation, the photogenerated electrons in the CB of CN-D transfer to the CB of CN-U by offset of 0.04 eV, whereas the photogenerated holes transfer from CN-U to CN-D driven by VB offset of 0.36 eV. Thus photogenerated electrons and holes can be separated effectively. For CN-MU heterojunction (Fig. 9b), the photo-induced electrons transfer from CN-U to CN-M driven by CB offset of 0.17 eV, while photogenerated holes cannot be transported from CN-M to CN-U as VB position of CN-M is more negative than that of CN-U. As the electrons are transferred from CN-U to CN-M, the photo-induced electrons and holes can also be separated. The charge separation and redistribution make the heterostructure into two different types (type I and type II). The potential differences drive higher separation efficiency and lower recombination rate in such metal free isotype heterostructures. Thereby, the photocatalytic performance of the g-C_3N_4/ g-C_3N_4 heterostructures is expected to be enhanced.

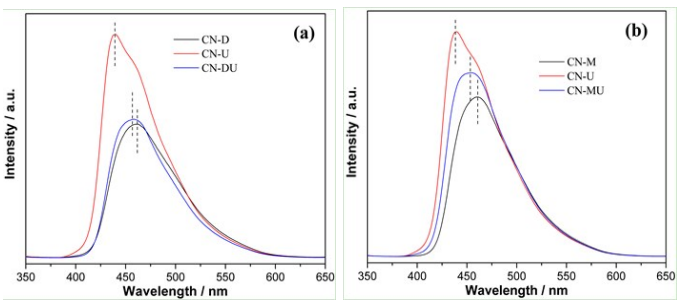

Fig. 10 Room temperature PL spectra of the samples (Excitation light source: 330 nm).

Fig. 10 shows the room temperature PL spectra of the samples. It can be seen that all the as-obtained samples present similar PL curves with emission peaks around 450 nm ascribing to the direct band transition. The slight deviation of the peak position is associated with the variation of band gap energy of these samples (Fig. 7). The CN-U is found to have a strong PL emission peak, while the PL peaks of CN-D and CN-M are relatively low due to the structural imperfection as shown in XRD. By electronic coupling of CN-U with CN-D (CN-M), the as-obtained CN-DU and CN-MU heterostructures exhibit low charge recombination. Thus, the intrinsic drawbacks of fast charge recombination in g-C_3N_4 can be solved by the construction of type I and type II isotype heterostructures. There numerous precursors for g-C_3N_4, and our method can be extended to construct other g-C_3N_4 based heterostructures by selecting appropriate composite precursors.

3.4. Visible-light photocatalytic activity and stability for NO removal.

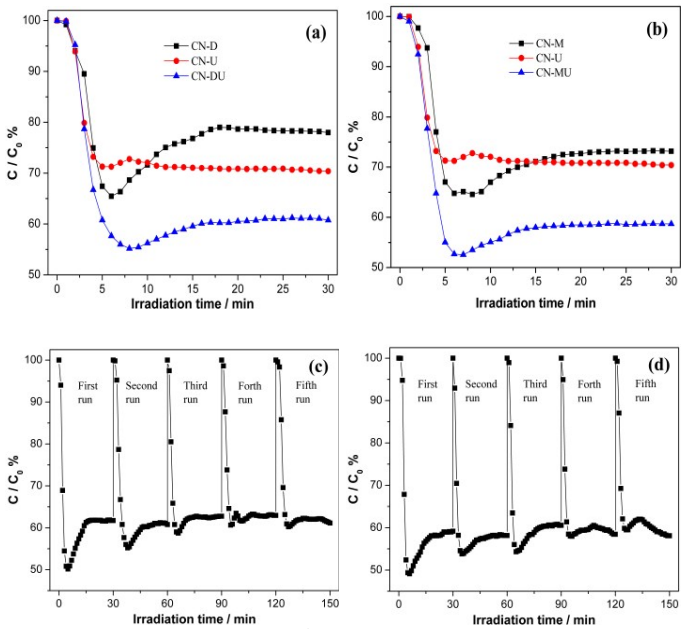

Fig. 11 Photocatalytic removal of NO over the samples and photocatalytic repeated runs over CN-DU and CN-MU under visible light irradiation.

The photocatalytic activity of CN-DU and CM-MU heterostructures was demonstrated for removal of NO under visible-light irradiation in a continuous reactor as shown in Fig. 11. Previous reports have shown that NO cannot be photolyzed only by illumination.[47] In the presence of photocatalyst and illumination, NO concentration (C/C_0%) is decreased rapidly as time goes by due to the photocatalysis (Fig. 11a and Fig. 11b). NO concentration first descends sharply and then tends to be steady after irradiation for 30 min. All g-C_3N_4 samples represent considerable visible-light photocatalytic activity for NO removal. It is significant to find that the NO removal ratios of CN-DU and CN-MU could reach up to 39.3 and 41.3%, respectively, which exceed these of the pristine g-C_3N_4 samples. The fact indicates that g-C_3N_4/g-C_3N_4 heterostructures with intimate electronic coupling plays a significant role in the enhancement of photocatalytic activity. The NO removal ratios of the samples are presented in Table 2.

Note that the NO removal ratios of the sample CN-MU (41.3%) is higher than that of the sample CN-DU (39.3%), which means the better photocatalytic performance of the type I than that of type II. This result can be explained by considering the working mechanism of type-I and type-II g-C_3N_4/g-C_3N_4 heterostructures under visible light irradiation. For CN-DU (type-II) heterojunction (Fig. 9a), the photogenerated electrons in the CB of CN-D transfer to the CB of CN-U and the photogenerated holes transfer from CN-U to CN-D, resulting in lowered redox potential of electrons and holes. For CN-MU (type-I) heterojunction (Fig. 9b), the photo-induced electrons transfer from CN-U to CN-M, while photogenerated holes cannot be transported from CN-M to CN-U. In this sense, the oxidative ability of the holes in g-C_3N_4 in type-I heterojunction can be preserved. Thus

type-I heterojunction exhibits higher oxidative ability and better photocatalytic performance over type-II heterostructure.

Not only the photocatalytic activity but also the photochemical stability is important for applications, which can be confirmed by repeated runs as shown in Fig. 11c and 11d.[62-64] It is obvious that under repeated irradiation, CN-DU and CN-MU still keep a high and relatively stable acvitity for NO removal without obvious deactivation.

The g-C_3N_4 is a metal free and earth-abundant photocatalyst that could work under visible light directly. There are many precursors for the synthesis of g-C_3N_4 with different band structures. By selecting suitable precursors, metal free type I and type II g-C_3N_4/g-C_3N_4 heterostructures can be successfully constructed with composite precursors. The present work could provide a new perspectives and general method for development of isotype g-C_3N_4 based heterostructures with high performance.

4. Conclusion

The g-C_3N_4 semiconductors prepared from different precursors have different band structure. By coupling g-C_3N_4 with distinctive band structure, different types of g-C_3N_4/g-C_3N_4 isotype heterostructures could be designed based on different band alignment patterns. Through thermal condensation of easily available composite precursors of dicyandiamide (melamine) and urea, Type I and Type II g-C_3N_4/g-C_3N_4 metal-free isotype heterostructures were successfully constructed. These heterostructures could effectively promote the separation of photo-induced electrons and holes, thus solving the intrinsic drawback of fast charge recombination of pristine g-C_3N_4. The Type I and Type II g-C_3N_4/g-C_3N_4 isotype heterostructures demonstrated highly enhanced visible light photocatalytic activity and stability for removal of ppb-level NO in comparison with g-C_3N_4 alone, which could be directly attributed to the promoted the charge separation resulting from the unique isotype heterostructures. As the precursors for g-C_3N_4 are abundant, the method can be extended as a general method. The present method for isotype heterostructured photocatalysts was facile and the samples could be easily produced in large scale. This novel isotype heterostructured photocatalysts with high performance could also be applied in other areas such as solar energy conversion, photosynthesis, photovoltaic, and biomedical areas.

Acknowledgements

This research is financially supported by the National Natural Science Foundation of China (51478070, 51108487), the Science and Technology Project from Chongqing Education Commission (KJ1400617).

*To whom correspondence should be addressed.
Phone: +86-23-62769785-605. Fax: +86-23-62769785-605.
E-mail: dfctbu@126.com

Notes and references

1 H. Tong, S. Ouyang, Y. Bi, N. Umezawa, M. Oshikiri and J. Ye, *Adv. Mater.*, 2012, **24**, 229.
2 S. Liu, J. Yu and M. Jaroniec, *M. Chem. Mater.*, 2011, **23**, 4085.
3 Y. Wang, X. Wang and M. Antonietti, *Angew. Chem., Int. Ed.*, 2012, **51**, 68.
4 Q. Xiang, J. Yu and M. Jaroniec, *Chem. Soc. Rev.*, 2012, **41**, 782.
5 X. Wang, S. Blechert and M. Antonietti, *ACS Catal.*, 2012, **2**, 1596.
6 F. Dong, S. C. Lee, Z. B. Wu, Y. Huang, M. Fu, W. K. Ho, S. C. Zou and B. Wang, *J. Hazard. Mater.*, 2011, **195**, 346.
7 Y. Zheng, J. Liu, J. Liang, M. Jaroniecc and S. Qiao, *Energy Environ. Sci.*, 2012, **5**, 6717.
8 F. Dong, H. T. Liu, W. K. Ho, M. Fu and Z. B. Wu, *Chem. Eng. J.*, 2013, **214**, 198.
9 G. Liu, P. Niu and H. Cheng, *ChemPhysChem.*, 2013, **14**, 885.
10 N. Tian, H. Huang, Y. He, Y. Guo and Y. Zhang, *RSC Adv.*, 2014, **4**, 42716.
11 X. Wang, K. Maeda, A. Thomas, K. Takanabe, G. Xin, J. Carlsson, K. Domen, M. Antonietti, *Nat. Mater.*, 2009, **8**, 76.
12 J. Hong, X. Xia, Y. Wang and R. Xu, *J. Mater. Chem.*, 2012, **30**, 15006.
13 Y. Liu, G. Chen, C. Zhou, Y. Hu, D. Fu, J. Liu, Q. Wang, *J. Hazard. Mater.*, 2011, **190**, 75.
14 J. Zhang, J. Sun, K. Maeda, K. Domen, P. Liu, M. Antonietti, X. Fua and X. Wang, *Energy Environ. Sci.*, 2011, **4**, 675.
15 J. Zhang, M. Zhang, G. Zhang and X. Wang, *ACS Catal.*, 2012, **2**, 940.
16 J. Zhang, X. Chen, K. Takanabe, K. Maeda, K. Domen, J. Epping, X. Fu, M. Antonietti and X. Wang, *Angew. Chem., Int. Ed.*, 2010, **49**, 441.
17 M. Bojdys, J. Müller, M. Antonietti and A. Thomas, *Chem.−Eur. J.*, 2008, **14**, 8177.
18 F. Dong, L. Wu, Y. Sun, M. Fu, Z. Wu and S. Lee, *J. Mater. Chem.*, 2011, **21**, 15171.
19 F. Dong, Y. Sun, L. Wu, M. Fua and Z. Wu, *Catal. Sci. Technol.*, 2012, **2**, 1332.
20 F. Dong, Z. Wang, Y. Sun, W. Ho, H. Zhang, *J. Colloid Interface Sci.*, 2013, **401**, 70.
21 Y. Cui, J. Zhang, G. Zhang, J. Huang, P. Liu, M. Antonietti and X. Wang, *J. Mater. Chem.*, 2011, **21**, 13032.
22 J. Xu, H. Wu, X. Wang, B. Xue, Y. Li and Y. Cao, *Phys. Chem. Chem. Phys.*, 2013, **15**, 4510.
23 Q. Xiang, J. Yu and M. Jaroniec, *J. Phys. Chem. C*, 2011, **115**, 7355.
24 S. Yan, S. Lv, Z. Li, Z. Zou, *Dalton. Trans.*, 2010, **39**, 1488.
25 J. Sun, Y. Yuan, L. Qiu, X. Jiang, A. Xie, Y. Shen and J. Zhu, *Dalton. Trans.*, 2012, **41**, 6756.
26 Y. Wang, X. Bai, C. Pan, J. He and Y. Zhu, *J. Mater. Chem.*, 2012, **22**, 11568.
27 N. Cheng, J. Tian, Q. Liu, C. Ge, A. Qusti, A. Asiri, A. Al-Youbi and X. Sun, *ACS Appl. Mater. Interfaces*, 2013, **5**, 6815.
28 J. Fu, B. Chang, Y. Tian, F. Xia and X. Dong, *J. Mater. Chem. A*, 2013, **1**, 3083.
29 L. Huang, H. Xu, Y. Li, H. Li, Xi. Cheng, J. Xia, Y. Xua and G. Cai, *Dalton Trans.*, 2013, **42**, 8606.
30 Y. Tian, B. Chang, J. Lu, J. Fu, F. Xi and X. Dong, *ACS Appl. Mater. Interfaces*, 2013, **5**, 7079.
31 Y. Sun, W. Zhang, T. Xiong, Z. Zhao, F. Dong, R. Wang, W. Ho, *J. Colloid Interface Sci.*, 2014, **418**, 317.
32 W. Zhang, Y. Sun, F. Dong, W. Zhang, S. Duan and Q. Zhang, *Dalton Trans.*, 2014, **43**, 12026.
33 Y. Wang, Z. Wang, S. Muhammad and J. He, *CrystEngComm*, 2012, **14**, 5065.
34 S. Kumar, A. Baruah, S. Tonda, B. Kumar, V. Shanker and B. Sreedhar, *Nanoscale*, 2014, **6**, 4830.
35 F. Wang, Y. Wang, X. Zhan, M. Safdar, J. Gong and J. He, *CrystEngComm*, 2014, **16**, 1389.
36 J. Zhang, Q. Xu, Z. Feng, *Angew. Chem., Int. Ed.*, 2008, **47**, 1766.
37 D. Scanlon, C. Dunnill, J. Buckeridge, S. Shevlin, A. Logsdail, S. Woodley, C. Catlow, M. Powell, R. Palgrave, I. Parkin, G. Watson, T. Keal, P. Sherwood, A. Walsh, A. Sokol, *Nat. Mater.*, 2013, **12**, 798.
38 X. Wang, Q. Xu, M. Li, S. Shen, X. Wang, Y. Wang, Z. Feng, J. Shi, H. Han and C. Li, *Angew. Chem., Int. Ed.*, 2012, **51**, 13089.
39 H. Wang, L. Zhang, Z. Chen, J. Hu, S. Li, Z. Wang, J. Liu and X. Wang, *Chem. Soc. Rev.*, 2014, **43**, 5234.
40 Z. Wang, Y. Liu, B. Huang, Y. Dai, Z. Lou, G. Wang, X. Zhang and X. Qin, *Phys. Chem. Chem. Phys.*, 2014, **16**, 2758.
41 S. Lo, T. Mirkovic, C. Chuang, C. Burda and G. Scholes, *Adv. Mater.*, 2011, **23**, 180.
42 Y. Wang, Q. Wang, X. Zhan, F. Wang, M. Safdar and J. He, *Nanoscale*, 2013, **5**, 8326.
43 M. Mikhailova, A. Titkov, Semicond. *Sci. Technol.*, 1994, **9**, 1279.
44 M. Hines, P. Guyot-Sionnest, *J. Am. Chem. Soc.*, 2003, **125**, 12567.
45 P. Reiss, J. Bleuse, A. Pron, *Nano Lett.*,2002, **2**, 781.
46 S. Lo, T. Mirkovic, C. Chuang, C. Burda, G. Scholes, *Adv. Mater.*, 2011, **23**, 180.
47 S. Kim, B. Fisher, H. Eisler, M. Bawendi, *J. Am. Chem. Soc.*, 2003,

125, 11466.
48 S. Ivanov, A. Piryatinski, J. Nanda, S. Tretiak, K. Zavadil, W. Wallace, D. Werder, V. Klimov, *J. Am. Chem. Soc*., 2007, **129**, 11708.
49 R. Xie, X. Zhong, T. Basche, *Adv. Mater.*, 2005, **17**, 2741.
50 F. Xu, V. Volkov, Y. Zhu, H. Bai, A. Rea, N. Valappil, W. Su, X. Gao, I. Kuskovsky, H. Matsui, *J. Phys. Chem. C*, 2009, **113**, 19419.
51 G. Wei, S. Forrest, *Nano Lett.*, 2007, **7**, 218.
52 R. Zeng, T. Zhang, J. Liu, S. Hu, Q. Wan, X. Liu, Z. Peng, B. Zou, *Nanotechnology*, 2009, **20**, 095102.
53 Osama M. Nayfeh, Cait Ni Chleirigh, John Hennessy, Leonardo Gomez, Judy L. Hoyt, and Dimitri A. Antoniadis, *IEEE Electr. Device L*., 2008, **29**, 1074.
54 R. Lu, C. Christianson, A. Kirkeminde, S. Ren, J. Wu, *Nano Lett.*, 2012, **12**, 6244.
55 B. Blackman, D. Battaglia, X. Peng, *Chem. Mater.*, 2008, **20**, 4847.
56 J. Zhang, M. Zhang, R. Sun and X. Wang, *Angew. Chem., Int. Ed.*, 2012, **51**, 10145.
57 F. Dong, Z. Zhao, T. Xiong, Z. Ni, W. Zhang, Y. Sun and W. Ho, *ACS Appl. Mater. Interfaces*, 2013, **5**, 11392.
58 Z. Zhao, Y. Sun and F. Dong, *Nanoscale*, 2015, **7**, 15.
59 G. Dong, Y. Zhang, Q. Pan, J. Qiu, *J. Photochem. Photobiol. C*, 2014, **20**, 33.
60 W. Zhang, Q. Zhang and F. Dong, *Ind. Eng. Chem. Res.*, 2013, **52**, 6740.
61 F. Dong, M. Ou, Y. Jiang, S. Guo and Z. Wu, *Ind. Eng. Chem. Res.*, 2014, **53**, 2318.
62 F. Dong, Z. Wang, Y. Li, W. Ho, S. Lee, *Environ. Sci. Technol.*, 2014, **48**, 10345.
63 T. Xiong, H. Huang, Y. Sun and F. Dong, *J. Mater. Chem. A*, 2015, **3**, 6118.
64. Z. Wang, W. Guan, Y. Sun and F. Dong, Y. Zhou and W. K. Ho, *Nanoscale*, 2015, **7**, 2471.